Spatial distribution of wave-by-wave overtopping behind vertical seawall with recurve retrofitting

S. Dong[1], S. Abolfathi[1*], M. Salauddin[2], J. M. Pearson[1]

[1] School of Engineering, University of Warwick, CV4 7AL, Coventry, UK

[2] Dooge Centre for Water Resources Research, School of Civil Engineering, and Earth Institute, University College Dublin, Dublin 4, Ireland

Abstract

Understanding the spatial distribution of wave overtopping water behind coastal protection structures is essential for assessing the safety level of coastal regions behind the coastal defences. The spatial distribution of wave overtopping volume determines the planning and arrangements of critical infrastructures (e.g., railways, roads and buildings) in coastal regions. This study presents a series of laboratory-scale physical modelling experiments to investigate the spatial distribution of wave overtopping volume behind plain vertical seawall and seawall with recurve retrofitting. The hydrodynamic conditions are designed to mimic both swell and storm sea conditions. Tests were conducted for a range of relative freeboard and empirical-based predictive equations were derived for both mean and extreme overtopping events under impulsive and non-impulsive wave conditions. Test results showed that overtopping impact hazard zone reduces up to 87% with the increase of relative freeboard (R_c/H_{m0}). The hazard zone for extreme overtopping events was found to be up to 3 times of the mean overtopping volumes. The effectiveness of recurve retrofitting on mitigating spatial distribution of wave overtopping were investigated with three recurve prototypes of varying overhang length and recurve's height. It was found that increase in overhang length provides higher reductions in the spatial distribution of hazard zone behind the wall and improve the climate resilience of the

seawall. The results highlight that recurve retrofitting is more effective in reducing the length of hazard zone under impulsive wave conditions. The findings of this study provide key data and predictive formulae for robust assessments of the hazard zones behind the key coastal defence infrastructures during mild and extreme climatic events.

Keywords: wave overtopping, vertical seawall, recurve wall, retrofitting, hazard-zone, spatial distribution, coastal resilience, coastal flooding, extreme climatic conditions

1. Introduction

Understanding the response of coastal defence infrastructures under different climatic conditions has been subject of research for many years. The majority of existing studies have focused on quantifying and predicting mean overtopping volumes from the coastal defences, as the main indicator for assessment of the safety level behind the defences. The significance of direct impact of overtopping events on the safety of vehicles, pedestrians and assets in coastal regions has received increasing attentions in recent years (Franco et al., 1994; Bruce et al., 2003; Allsop et al., 2005a; Bruce et al., 2005; Van der Meer and Bruce, 2014; Salauddin et al., 2017; Salauddin and Pearson, 2018 and 2020). Knowledge of the spatial distribution of wave overtopping from defence infrastructures is key to understand the safe zone behind coastal defences. The existing predictive tools for determining the spatial distribution of overtopping are based on empirical formulae, derived from the mean overtopping volumes. However, severe post overtopping hazards more commonly occur from extreme individual wave overtopping events.

Jensen and Sorensen (1979) undertook experimental investigations on the spatial distribution of overtopping water behind the rubble mound breakwaters and derived empirical equations to describe the intensity of overtopping water as a function of the distance behind the defence.

48 Bruce et al. (2005) and Pullen et al. (2006), studied the spatial distributions of overtopping
49 waves behind vertical seawalls by undertaking field and laboratory-scale investigations,
50 highlighting the significance of wind speed in the spatial distribution of overtopping. Pullen
51 et al. (2009) showed that the shape of spatial distribution of overtopping can be described as a
52 function of the wind speed and incident wave characteristics.

53 The existing data on spatial distribution of overtopping waves behind the seawalls are mainly
54 focused on mean overtopping water, which help understanding the intensity of the mean
55 overtopping over the duration of a typical storm. However, the characteristics of spatial
56 distribution of overtopping form an extreme individual overtopping wave is still not well
57 understood. For rubble mound breakwaters, Andersen and Burcharth (2005) and Andersen et
58 al. (2009) undertook field and laboratory studies and proposed empirical relations suggesting
59 spatial distribution can be predicted as a function of wave steepness.

60 Peng and Zou (2011) simulated the spatial distribution of overtopping water from both sloping
61 and vertical structures using a RANS-VOF numerical model with standard $k-\varepsilon$ turbulence
62 closure model. The findings of Peng and Zou (2011) confirm the predictions formulated by
63 Andersen et al. (2009) and Pullen et al. (2009), and show that the maximum individual
64 overtopping event travels further than the mean overtopping distribution, although the overall
65 distribution profile had similar characteristics. Despite the recent advancement in
66 understanding spatial distribution of wave overtopping behind coastal defences, there are little
67 information available on the travel distance of extreme individual overtopping events.

68 The combined effects of climate change and sea-level rise (IPCC, 2018), increase the frequency
69 of extreme climatic events which can lead to severe overtopping hazards (Dong et al., 2020a,
70 b; Abolfathi et al., 2016, 2018, 2020; Cheon and Suh, 2016; Chini and Stansby, 2012). The
71 reduced freeboard of existing defences due to sea-level-rise together with aging coastal defence

infrastructures can reduce the level of protection they provide against extreme climatic events and can potentially lead to catastrophic floods. Therefore, in recent years several research projects focused on enhancing climate resilience of existing defences through retrofitting (e.g., Pearson, 2010; Van Doorslaer and De Rouck, 2011; Dong et al., 2018 and 2020a; Salauddin et al., 2020a, b). Despite extensive research has been carried out to understand wave runup and mean overtopping attenuations from recurve walls, very limited information is available on the post overtopping performance of recurves and spatial distribution of overtopping (Kortenhaus et al., 2003; Pearson et al., 2004).

This paper presents comprehensive laboratory-scale physical modelling investigations on the spatial distribution of overtopping volumes at plain vertical and recurved seawalls under both impulsive and non-impulsive conditions. The spatial distributions of extreme overtopping events are compared with mean overtopping volume. Physical modelling experiments for recurve walls include three size of recurves with varying height and overhang length to better understand the role of geometrical properties of recurves on the distributions of overtopping behind the seawall. Using data from physical modelling, this study develops reliable physics-based predictive tools for spatial distribution of wave-by-wave and overall overtopping events in an overtopping sequence of waves.

2. Previous work

2.1 Existing empirical-based predictive relations

Wave overtopping processes on vertical walls are complicated function of non-linear wave hydrodynamics, structural configurations, wave-structure interactions and relative crest freeboard of structures. Understanding the influence of wave breaking phenomena and runup at seawall, during highly turbulent storm conditions, add to the complexity of the overtopping processes at the seawall. Bruce et al. (2005) and Pullen et al. (2009) using data from laboratory

and field measurements, investigated the spatial distribution of overtopping from composite and steep structures and suggested that the spatial distribution of overtopping water can be described as the relationship between overtopping volumes and the travel distance of overtopping waves behind the defence structure (Pullen et al., 2006). To minimise the scatters in results, the overtopping discharge is normalised by the total discharge q, and travel distance is normalised by the offshore wavelength L_0. Eq. (1) presents Pullen et al. (2006) empirical-based prediction for spatial distribution of overtopping:

$$q^* = \frac{x\prime}{q_{total}} = e^{(-k(x'))} \quad [1]$$

where q^* presents the ratio of discharge lands after the normalised overtopping distance x' to the total discharge ($q_{x\prime}/q_{total}$), x' is the normalised overtopping distance defined as $x'=x/L_0$, k is the empirical coefficient, which is set to 29 when no wind effects are considered. The k coefficient also controls the shape of spatial distribution of overtopping. Figure 1 illustrates the parameters used in Eq. (1) for describing the spatial distribution of overtopping water. Eq. (1) has been used for analysing the spatial distribution of both mean overtopping volume and extreme individual wave events (Pullen et al., 2006).

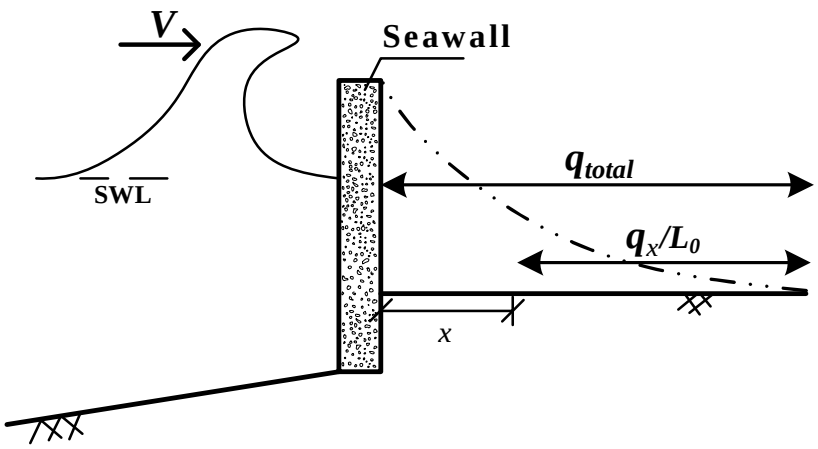

Figure 1 – Schematic of parameters used in describing spatial distribution of wave overtopping. The q_{total} represents the total overtopping discharges, q_x is the discharge in the distance of x behind the seawall, L_o is the offshore wavelength, v represents the direction of incident weaves.

2.2 Wind effects

In order to provide a robust prediction of the spatial distribution of overtopping in real-life field conditions, it is very important to understand the influence of wind effects on wave overtopping. Previous work confirmed increase on the overtopping discharge under shore-ward wind effects (de Waal et al., 1997; Ward et al., 1996; Pullen et al., 2006). Pullen et al. (2006) investigated the influence of wind on overtopping and proposed a revised empirical coefficient k as a function of wind speed, Vw (Eq. 2):

$$k = 29e^{(-0.03V_w)} \quad [2]$$

The empirical coefficient k in Eq.1 and Eq. 2 is conservatively determined based on field and laboratory-based measurements following the largest travel distance in all measured conditions, resulting in a conservative engineering design (Pullen et al., 2009). However, the predictions from Eq. (1) and Eq. (2) noticeably overestimate spatial distribution of overtopping, especially immediately behind the seawall structure. More research and data are needed in order to better understand the post overtopping processes and optimizing the existing predictive tools.

2.3 Scale effects

According to field and laboratory measurements, Andersen et al. (2009) and Pullen et al. (2009) concluded that for impermeable sloping and vertical structures, scale effects on the spatial distributions of overtopping waves are negligible. However, difficulties in replicating field-based wind effects in laboratory experiments, can lead into scale difference in air and spray effects. The scale difference in the interactions between wind and spray can lead to differences

in overtopping measurements between laboratory and field conditions. Therefore, a scaling effects should be considered in prediction of spatial distribution of overtopping when wind effects is considered.

2.4 Extreme overtopping events

Previous studies highlight the importance of maximum individual overtopping events for assessing hazard level behind the coastal defences, given that the discharge of extreme individual overtopping events can be significantly larger than mean overtopping discharge (Allsop et al., 2005b; Besley et al., 1998). Similarly, the affected area of overtopping water for extreme individual overtopping events can be much larger than mean overtopping and therefore understanding post overtopping processes for extreme events is key to protect people and critical infrastructures in coastal region against overtopping hazards (Andersen and Burcharth, 2007; EurOtop, 2018).

The majority of existing data focus on the spatial distribution of mean overtopping discharge, while limited information is available for extreme overtopping events. Andersen et al. (2009) investigated post overtopping processes for rubble mound breakwater and demonstrated similarities exist between spatial distributions characteristics of mean and extreme overtopping events. No significant deviations were observed between spatial distributions of the wave-by-wave and mean overtopping events for the case of rubble mound breakwater (Andersen et al., 2009). However, Peng and Zou (2011) using numerical simulations, showed the difference between the spatial distribution of the largest overtopping event and the mean overtopping volume.

In recent years, application of numerical modelling in understanding complex wave-structure interactions and the influence of nearshore processes on the performance of coastal defence structures has received more attention (e.g., Yeganeh-Bakhtiary et al., 2017 and 2020;

Abolfathi et al., 2017 and 2018; Fitri et al., 2019; Liu et al., 2020a,b). Peng (2010) adopted RANS-VOF modelling technique with $k-\varepsilon$ turbulence closure to study spatial distributions of overtopping water. Peng (2010) numerical results showed good agreement with Andersen et al. (2009) data for the sloping structures, and Pullen et al. (2009) measurements for vertical seawall. Numerical studies also illustrated that overtopping water in extreme events affects larger coastal area in comparison to the time-averaged spatial distributions for both sloping and vertical seawalls (Peng, 2010).

Analysis of existing data on spatial distributions of overtopping highlights the importance of high-resolution measurement of overtopping volumes behind the seawall to have in-depth understanding of post overtopping hazards. For laboratory and field-based studies, appropriate design of overtopping measurement system is recommended to capture high-resolution detailed changes in overtopping discharges with the distance from the seawall. However, to this date, no research investigated the effects of overtopping measurement resolutions on the spatial distribution of mean and wave-by-wave overtopping water.

3. Experimental Set-up

The physical modelling tests were undertaken in a two-dimensional wave flume at Warwick Water facility, the University of Warwick. The flume has dimensions of 22.0 (L) × 0.6 (W) × 1.0 (H) m with a 1:20 smooth foreshore beach slope made from glass (Figure 2a). The flume is equipped with a piston-type wave generator and an active wave absorption system (AWAS). Experiments were carried out with a vertical seawall fixed at a distance of 12.21m from the wave paddle. The recurve retrofitting structure was placed in front of the seawall crest.

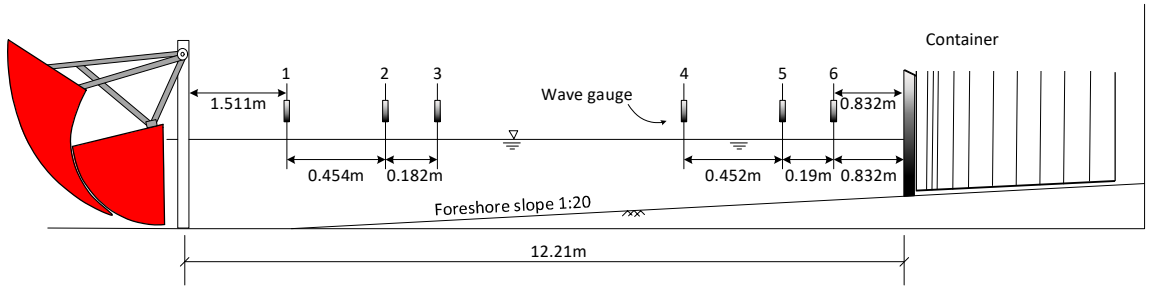

(a)

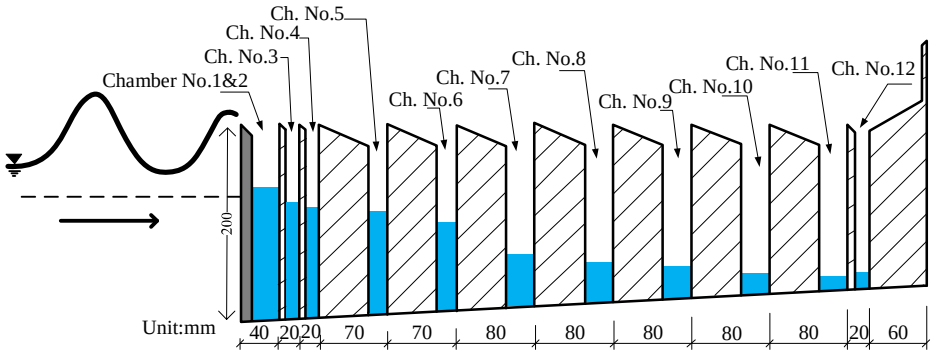

(b)

Figure 2 – Schematic of (a) the 2D wave flume with active absorption piston-type wave generator, experimental setup and location of wave gauges (adopted from Dong et al., 2020b) and (b) container designed for the measurement of spatial distribution of wave overtoppings from the seawall

In order to control and minimize the uncertainties in experimental results, each test case was consisted of approximately 1000 pseudo-random waves based on the JONSWAP spectrum with γ factor of 3.3. The tests were designed at a length scale of 1:50. The characteristics of incident and reflected waves were determined using two sets of three wave gauges which were placed close to paddle and seawall, respectively. The distance between each set of three gauges was determined based on the Least-Square Method described by Mansard and Funke (1980). Additional tests were carried out in the 'bare' flume without the structure in place to measure the inshore wave conditions with limited influence of reflection from the seawalls, as adopting the typical wave measurement techniques in small-scale wave flume investigations, e.g.,

Pearson et al., 2002; Dong et al., 2018; Salauddin et al., 2020b, 2021. To avoid any uncertainty which may arise in the measurement of wave conditions, this study adopts the wave conditions determined from calibration conditions ('bare flume'). The overtopping measurements was recorded continuously and without any interruption during all the tests.

Table 1 summarizes the details of wave conditions and seawall configurations tested within this study. The experiments were designed to incorporate significant wave height ranging between 0.041m and 0.105m, and wave periods ranging from 0.8s – 1.75s. This study investigated overtopping for a range of wave steepness ranging from 0.016 to 0.068 under both swell and storm wave conditions. To provide comprehensive dataset representative of a range of operational conditions, dimensionless freeboard from 0.86 to 3.2 were tested in this study.

Table 1 – Nominal wave conditions used for the physical modelling tests

Height of seawall [m]	water depth [m]	Nominal wave period [s]	Significant wave height [mm]
0.21	0.07	0.80	60
		0.90	78
		0.95	97
		1.20	59
		1.50	65
		2.00	69
	0.09	0.80	66
		0.90	78
		0.95	79
		1.00	62,68,92
		1.10	80
		1.20	72,117
		1.25	67,74
		1.35	75
	0.11	0.85	73
		0.90	76
		0.95	80
		1.00	95
		1.10	105
		1.15	118
		1.35	77
		1.42	79
		1.80	79,85

0.31	0.15	0.90	58,61,64,72,76
		1.00	43
		1.20	50,54
	0.18	0.95	78
		1.00	49,83
		1.10	71
		1.20	57
		1.35	63,71
		1.50	48,51
	0.21	0.90	71
		0.95	72
		1.00	87
		1.10	85
		1.20	60,74
		1.25	54
		1.35	68
		1.50	57

A multi-chamber container was designed for capturing detailed and high-resolution information on the spatial distribution of overtopping water as well as mean overtopping volume. The chamber was fixed behind the vertical seawall for all test configurations. Figure 2b shows the design details of the multi-chamber overtopping collection system used in the study. The container is designed to have higher resolution immediately after the seawall (i.e. smaller distance between the chambers), and as moving further from the seawall distance between the chambers were increased. The top of each chamber's wall was made into a slope with a sharp edge in order to minimize the overtopping volumes jumping into adjacent chambers. A LED band is mounted across the crest of all chambers, which is built to light up chambers and help controlling water level in chambers. The overtopping measurement chambers were designed to ensure high-resolution data especially in the area close to the seawall crest to address existing gap of knowledge in terms of assessing hazards immediately after the seawall. The summation of the overtopping discharge (q_x) measured in individual chamber is the total overtopping discharge (q_{total}) measured behind the seawall.

223 The influence of recurve geometrical shape and size on the distribution of wave overtopping
224 and hazard zone behind the wall were investigated using three recurve sizes in the physical
225 modelling experiments. The test cases with recurve retrofitting of similar overhang length and
226 height, named as Small Recurve (SR), is considered as base-case for comparing the
227 performance of other retrofitting cases including Long Recurve (LR) and High Recurve (HR).
228 The dimensions of recurve retrofitting tested in this study are presented in Figure 3. Prior to
229 testing recurve walls, overtopping discharge and its spatial distribution were recorded at the
230 plain vertical seawall for all the hydrodynamics conditions described in Table 1. Investigations
231 are undertaken for the influence of both hydrodynamics and geometrical properties of
232 retrofitting on the spatial distribution of hazard zone behind the seawall. This study has also
233 investigated the response of recurve walls against steep and smooth incident waves.

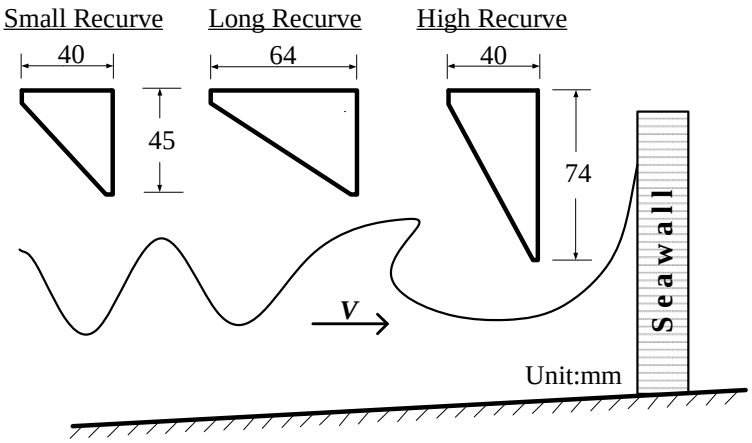

Figure 3 – Schematic of the three recurve walls tested in this study

4. Results and Discussions

4.1 Overtopping discharges

The mean overtopping discharge is a key indicator for assessing the hazards from wave overtopping in coastal regions. Several studies have been undertaken to derive robust predictive relations for mean overtopping discharge from vertical seawalls (e.g., Besley, 1999; Franco et al., 1994; Allsop et al., 2005b; Goda, 2009; Van der Meer and Bruce, 2014; Dong et al., 2020a; O'Sullivan et al., 2020; Salauddin and Pearson 2019, 2020; Salauddin et al., 2020a). The mean overtopping discharge measured for the plain and recurve seawalls in this study are compared to EurOtop (2018) predictions for both impulsive and non-impulsive wave conditions.

Figure 4 shows the measured mean overtopping discharge from plain vertical seawall for the case of impulsive and non-impulsive waves. The comparison of measured overtopping rates with the empirical-based predictions indicates robust predictions from EurOtop (2018) formulae. However, for the case of non-impulsive waves and seawall configurations with large freeboard, a noticeable underestimation of EurOtop (2018) predictions is observed (Figure 4b). The deviations between measurements and EurOtop (2018) predictions in Figure 4b, are particularly larger for the test cases with small wave steepness and for those configurations with higher relative freeboard. Further analysis of the results presented in Figure 4b shows that

existing prediction formulae tends to underestimate the mean overtopping discharges for the cases with h_* lower than 0.3. Besley et al. (1998), reported similar trend in their measurement for non-impulsive wave conditions. The physical modelling results for the cases of plain vertical seawall are used as reference cases in this study.

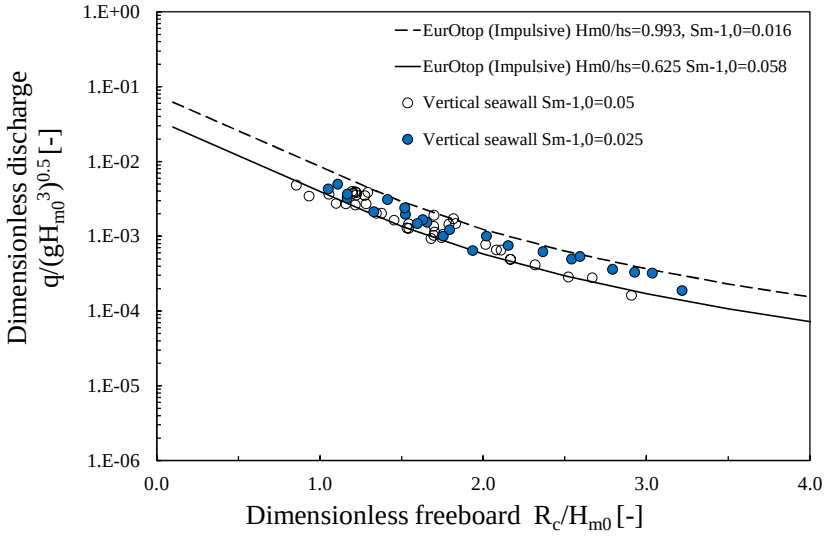

(a)

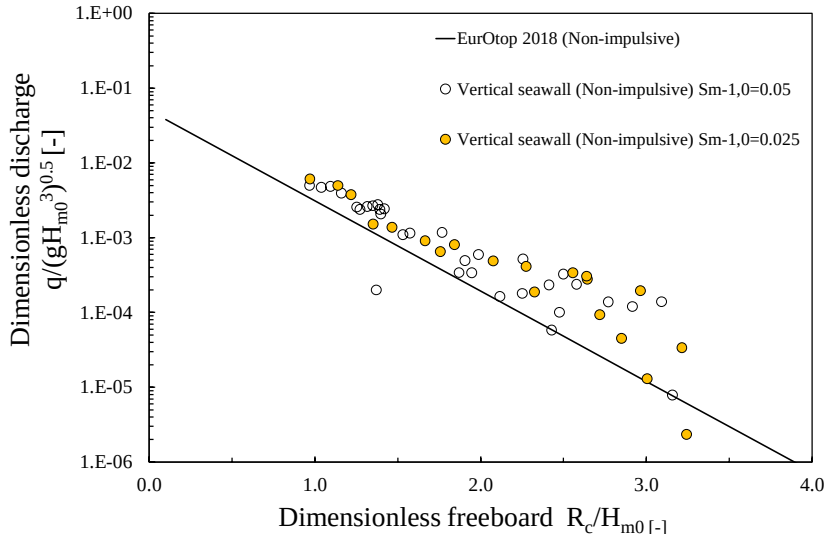

(b)

Figure 4 – Mean overtopping discharge on plain vertical seawall for (a) Impulsive wave conditions and, (b) Non-impulsive wave conditions

260 ### 4.2 Spatial distribution of the wave overtopping volume

261 #### 4.2.1 Comparison with existing predictions

262 Pullen et al. (2009) suggested empirical-based equations for prediction of spatial distributions
263 of wave overtopping behind plain vertical seawalls (Eq. (1)). Figure 5 compares the measured
264 spatial distribution of wave overtopping from this study with the predictions from Eq. (1), for
265 the cases with plain vertical seawall and without considering the wind effects. Figure 5 (a-d)
266 present the measured spatial distribution of the mean, the highest two and, the extreme
267 overtopping events. The extreme overtopping events in Figure 5 is defined as the average
268 distribution of the highest five overtopping events, to minimise the uncertainties of taking an
269 individual overtopping event as extreme event. The distributions of overall and extreme
270 overtopping events measured for the cases with large freeboard are smaller than the predictions
271 from Pullen et al. (2009) formulae, indicating existing empirical-based predictions
272 overestimate the travel distance of overtopping water, especially for the cases with high
273 freeboard (Dong and Pearson, 2018). Pullen et al. (2009) highlights that 90% of overtopping
274 water lands behind the seawall within a distance of 0.08 of incident wavelength. The
275 measurements from this study show that similar volume of overtopping water lands within a
276 distance of $0.04 \times L_0$ of incident waves. However, over-prediction in spatial distribution of
277 overtopping from Pullen et al. (2009) formulae reduces and become negligible when freeboard
278 approaching 1.

279

Review of the findings from Pullen et al. (2006) and Pullen et al. (2009) studies show that their empirical formula for spatial distribution of overtopping was derived considering the most conservative scenarios of affected area behind coastal defences. The overtopping travel distances recorded in this study from the physical modelling tests show significant deviations from the conservative predictions recommended by Pullen et al. (2009), especially for the cases with large freeboard. Despite conservative predictions of spatial distribution of overtopping may not be critical for the coastal regions with farmlands or flat field, these predictions can have significant consequences for the cases with limited space in coastal area, such as a railway on the cliff, or those densely populated regions with high socioeconomic values. Therefore, the influence of freeboard on the spatial distribution should be carefully considered when robust predictions of overtopping spatial distributions is necessary.

To provide reliable assessments of the risks of damages, caused by wave overtopping in coastal areas, high resolution data on spatial distribution of significant overtopping events are required. Figure 5 improves the existing knowledge of spatial overtopping distribution immediately after the seawall by presenting high-resolution measurements of overtopping distributions near the parapet region behind the seawall. The spatial distribution of overtopping in Figure 5 is shown as a function of square-root of travel distance of $x/L_{m\text{-}1,0}$. The data presented in Figure 5 (a-d), covers both impulsive and non-impulsive wave conditions and present an improved understanding of the spatial distribution of 95% of overtopping discharges behind the coastal defences. In Figure 5, the high-resolution spatial distribution of the mean overtopping volume landing within the distance of 0.1 wavelength is presented. The results presented in Figure 5 indicate that less than 3% of the mean overtopping volume travels beyond the distance of 0.1 of wavelength.

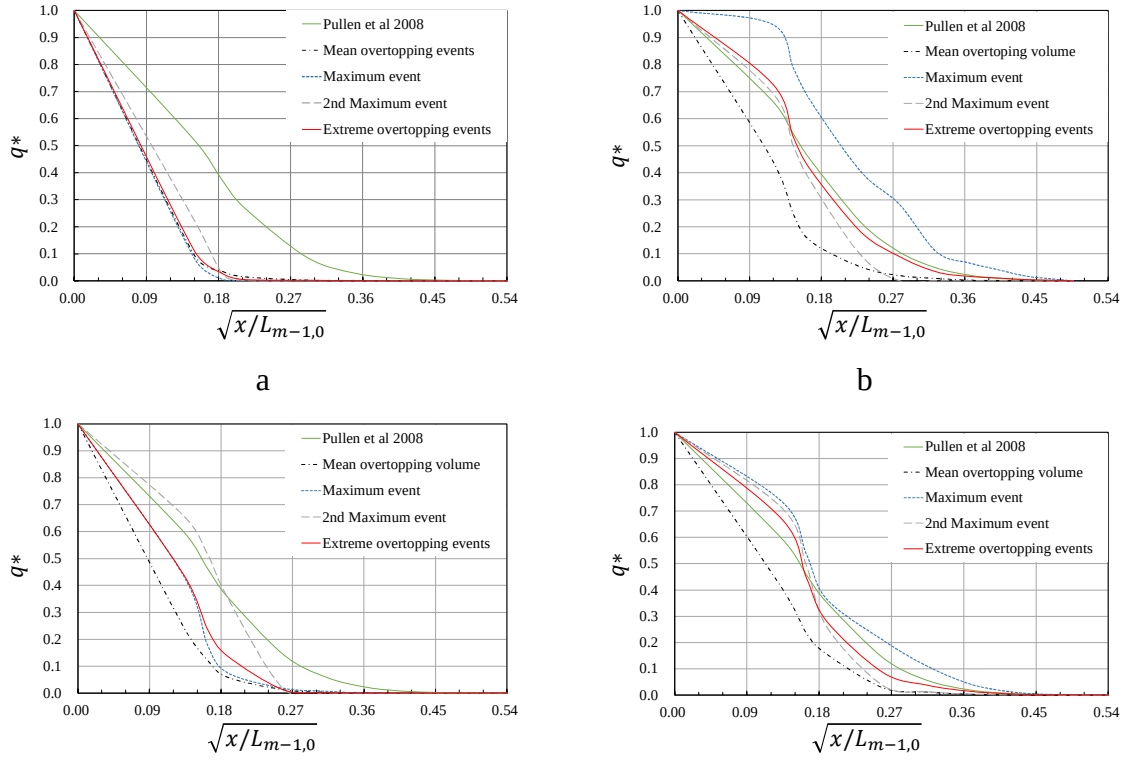

Figure 5 – The spatial distribution in near parapet region behind the plain vertical seawall - (a) R_c/H_{m0}=1.755 (Impulsive), (b) R_c/H_{m0}=1.109 (Impulsive), (c) R_c/H_{m0}= 2.273 (Non-impulsive), (d) R_c/H_{m0}= 1.138 (Non-impulsive). [$q^*=q_{x/Lm\text{-}1,0}/q_{total}$]

Despite Pullen et al. (2009) empirical relations led to over predictions of spatial distribution of overtopping near the parapet region, the shape of spatial distribution from empirical relation is similar to the shape of spatial distribution measured in this study. Thus, this study adopts the same methodology outlined in Pullen et al. (2009) to derive new and improved predictive relations for the spatial distribution of both overall and extreme overtopping events. In Eq. (1), the shape of the spatial distribution is determined by the empirical parameter *k*. Figure 6a and b show differences in the shape of spatial distribution, with the spatial distribution of overtopping waves further from the seawall. The data obtained from the measurements will be further analysed in the next section to investigate the possible reasons for the differences in the

316 shape of the spatial distribution of overtopping volume across the tested configurations and
317 wave conditions.

318 **4.2.2 Mean overtopping events**

319 On sloping structures, Peng (2010) and Andersen et al. (2009) reported influences from relative
320 freeboard to the shape of spatial distribution. Lower freeboards are associated with longer
321 travel distance of overtopping water for sloping structures. Identical phenomenon is also
322 observed from the physical modelling data on the vertical seawalls. Comparison of the spatial
323 distribution of overtopping between Figure 5a and 5b highlights the significance of crest
324 freeboard level on the shape of overtopping spatial distribution immediately behind the wall.
325 In Figure 5, for the impulsive wave conditions, when $R_c/H_{m0}=1.755$, 85% of overtopping water
326 locates within a distance of 0.02 wavelength. Meanwhile, by reduction of R_c/H_{m0} to 1.109, the
327 travel distance of 85% overtopping water increases to 0.031 wavelength. Moreover, comparing
328 Figure 5a and b, the travel distance of the mean overtopping discharge increases 1.5 times on
329 plain vertical seawall due to the reduction in freeboard. Analysis of physical modelling data in
330 this study shows that the shape parameter (k) in the empirical predictions of spatial distribution
331 of overtopping is changing as a function of the relative freeboard R_c/H_{m0}.

332 Figure 6 plots the spatial distribution shape parameter k against the relative freeboard for the
333 plain vertical seawall under impulsive and non-impulsive conditions. Analysis of data
334 presented in Figure 6 shows that an exponential function of relative freeboard can approximate
335 the k value with good precision. The relationship between k and relative freeboard for the tests
336 with impulsive wave conditions, is empirically determined and presented in Eq. 3 with the root
337 mean square error (RMSE) of 0.075.

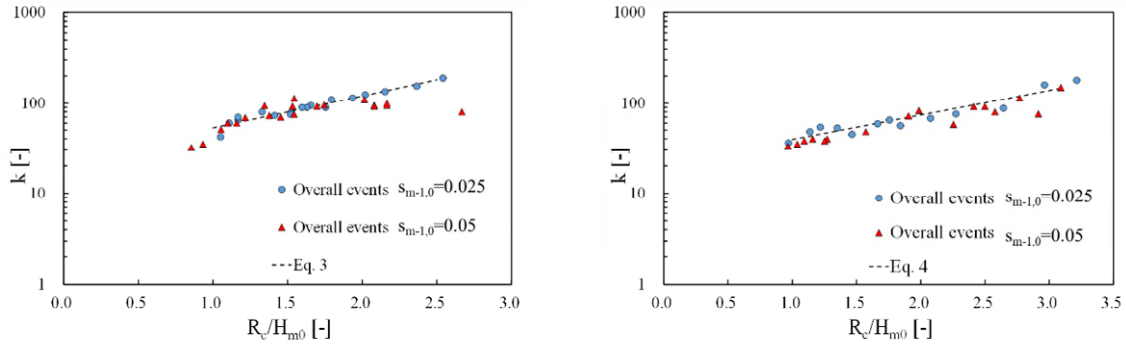

a b

338 Figure 6 – Relationship between k and R_c/H_{m0} for the spatial distribution of mean overtopping
339 discharge (a) Impulsive test conditions (b) Non-impulsive test conditions

340 For the non-impulsive overtopping events, crest freeboard has similar significance in
341 determining the shape of spatial distribution of overtopping waves in the landward area behind
342 the seawall. Figure 5d shows that for non-impulsive waves, over 85% of the overtopping water
343 lands within a distance of 0.45 offshore wavelength behind the crest of structure. However, this
344 distance of 0.45 offshore wavelength reduces in Figure 5c due to the increase in R_c/H_{m0}. The
345 comparison between Figure 5c and 5d shows that the spatial parameter k can also be described
346 with an exponential function of relative freeboard, as seen in Figure 6b. The parameter k is
347 empirically derived and presented in Eq. 4, with the RMSE of 0.12.

348 $$k = 23e^{\frac{0.82R_c}{Hm0}} \qquad \text{Impulsive conditions } 0.9 < R_c/H_{m0} < 2.5 \qquad [3]$$

349 $$k = 21e^{\frac{0.63R_c}{Hm0}} \qquad \text{Non-impulsive conditions } 1.0 < R_c/H_{m0} < 3.0 \qquad [4]$$

350 **4.2.3 Extreme overtopping events**

351 The significance of extreme overtopping events in the assessments of coastal areas behind
352 defence structures has been emphasised by many researchers and design guidelines, over the
353 years. Previous studies investigated spatial distribution on maximum overtopping events on
354 sloping structures and reported similarities between the travel distance of maximum
355 overtopping events (see Andersen et al. 2009). Numerical investigations highlighted that the

maximum overtopping events can travel further than the mean overtopping (Peng and Zou, 2011). This study investigated the influence of extreme overtopping events on plain vertical seawall. The results confirmed that extreme overtopping events generally travels further than the mean overtopping measurements. Further analysis of Figure 6 shows that the *k* parameter for both total distribution and the individual overtopping events follows the exponential relation, meaning that the value of *k* for the extreme overtopping events can also be approximated as an exponential function of relative freeboard (Figure 7).

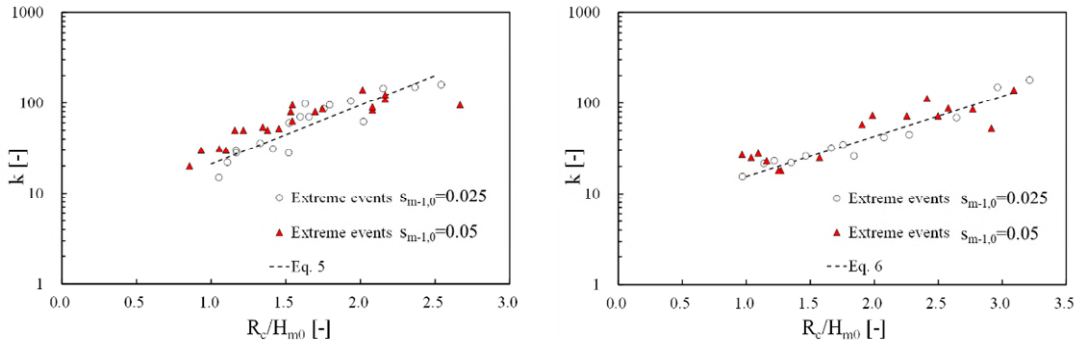

a b

Figure 7 – Relationship between *k* and R_c/H_{m0} for the average spatial distribution of the extreme overtopping events with largest 5 discharges. (a) Impulsive test conditions (b) Non-impulsive test conditions.

The spatial shape parameter *k* for extreme overtopping events are derived based on physical modelling data and described in Eq. 5 and 6, for impulsive and non-impulsive wave conditions, respectively. The RMSE for Eq. 5 and 6 are determined to be 0.11 and 0.14, respectively.

$$k = 4.7e^{1.5R_c/H_{m0}} \quad \text{Impulsive conditions} \quad 0.9 < R_c/H_{m0} < 2.5 \qquad [5]$$

$$k = 5.6e^{1.02R_c/H_{m0}} \quad \text{Non-impulsive conditions} \quad 1.0 < R_c/H_{m0} < 3.0 \qquad [6]$$

To highlight the influence of R_c/H_{m0} on the spatial distribution of hazard zone behind the seawall, the affected range of significant overtopping discharge with various R_c/H_{m0} were

analysed. Figure 8 shows the relationship between the dimensionless travel distance of 85% mean overtopping discharge with relative freeboard R_c/H_{m0}, indicating that overtopping travel distance falls sharply as the crest freeboard increases. A reduction of up to 87% is observed in travel distance when the relative freeboard R_c/H_{m0} increases from 0.85 to 2.5. The parametric analysis confirms the significance of freeboard level in determining the wave overtopping hazard zone, and the reduction in travel distance due to the increase of freeboard is quantified.

.

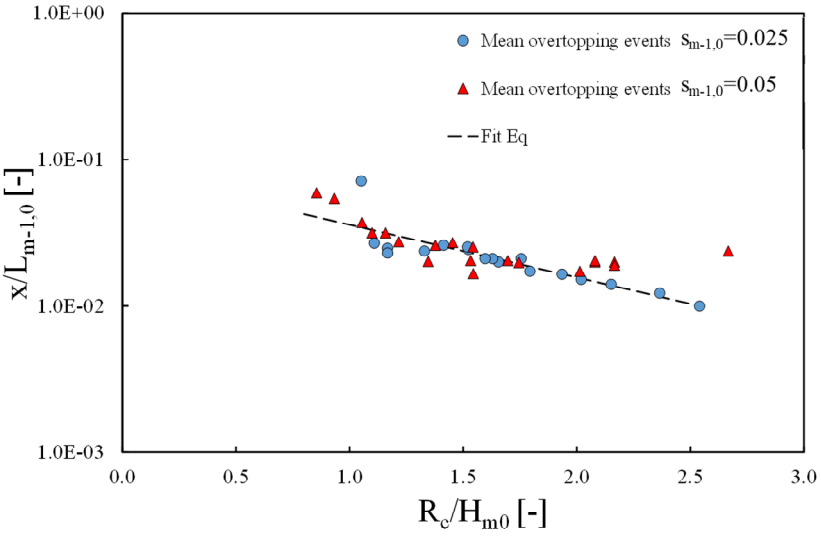

Figure 8 – The variations in travel distance ($x/L_{m\text{-}1,0}$) of 85% mean overtopping discharges by changes in dimensionless freeboard (R_c/H_{m0})

4.2.4 Influence of wave steepness

Despite the obvious impact of wave characteristics on the wave-structure interactions, dynamic response of defence infrastructure to incident wave attack and the consequent wave overtopping, the influence of key underlying wave climate parameters, such as wave steepness, on the spatial distribution of wave overtopping is not fully understood yet. Previous studies show reduction of the mean overtopping discharge with an increase in wave steepness (Besley et al., 1998; Goda, 2000; Van der Meer and Bruce, 2014; Dong et al., 2020a). Results from this investigations the underlying physical processes of wave overtopping, show that the wave

391 impulsiveness parameter (h_*) can influence the throw-up velocity during the overtopping
392 processes which can directly impact the spatial distribution of hazard zone behind seawalls
393 (Bruce et al., 2003). This study hypothesised that the wave steepness can alter the trajectory of
394 overtopping waves, given that the shape of incident waves can significantly change the travel
395 distance of overtopping water behind the defence structure.

396 The measurements of overtopping from plain vertical seawall show that increase in wave
397 steepness values (from 0.025 to 0.05) for the non-impulsive wave conditions is not influencing
398 the *k* parameter (Figure 6 and Figure 7). However, a clear exponential correlation between all
399 measured *k* with R_c/H_{m0} is observed for the case of non-impulsive test conditions. Similar
400 findings are observed for tests with impulsive wave conditions when $R_c/H_{m0}<2.0$. For those
401 tests with R_c/H_{m0} larger than 2.0, the wave steepness values play a more distinctive role in
402 influencing *k* values, where *k* for those conditions with large wave steepness remains
403 approximately constant, and for the case of small wave steepness, *k* has increased exponentially
404 with R_c/H_{m0}.

405 Pullen et al. (2009) proposed normalising the overtopping travel distance by wavelength for
406 the individual overtopping scenarios. This study confirms the findings of Pullen et al. (2009),
407 and given that the non-normalised wave overtopping travel distance is influenced by both
408 wavelength and wave period, wave steepness parameter is proposed as effective index to
409 evaluate post overtopping processes of individual overtopping cases. The physical modelling
410 measurements show that longer wave periods lead to an increase in the *k* value of the spatial
411 distribution of wave overtopping, even if the overall travel distance is not changed.

412 To evaluate the effects of incident wave steepness on the spatial distribution of hazard zone
413 behind the seawall, the measured spatial distribution of overtopping volume is described as a
414 function of absolute travel distance (x) instead of being normalised by offshore wavelength,

415 i.e., $x/L_{m-1,0}$. Figure 10 presents the observed k values for all the test configurations against the
416 relative freeboard. The dimensionless k values derived based on Pullen et al. (2009)
417 methodology are shown in Figure 9(a), whereas the proposed new dimensional spatial
418 parameter k values are presented in Figure 9(b). Data in Figure 9 demonstrate that both
419 dimensional and dimensionless values of k increase exponentially with the relative freeboard
420 of the seawall structure. However, dimensional values of k in Figure 9 (b) are relatively smaller
421 than those reported for non-dimensional cases in Figure 9 (a) and, they are also more scattered
422 across all the test cases which can be associated with the lack of normalising processes. The
423 results shown in Figure 9 (b) reveal the impacts of wave steepness on the variation of k
424 parameter. The analysis of the measured data show that the k values correspond to the large
425 wave steepness of $s_{m-1,0} = 0.05$, are overall greater than those determined for test configurations
426 with small wave steepness conditions. While the deviations in k parameter caused by wave
427 steepness are not remarkable, they imply that the influence of wave steepness in the spatial
428 distribution of overtopping is not negligible. As the freeboard increases, the difference of
429 distribution of overtopping volume between large and small wave steepness conditions
430 becomes limited.

431

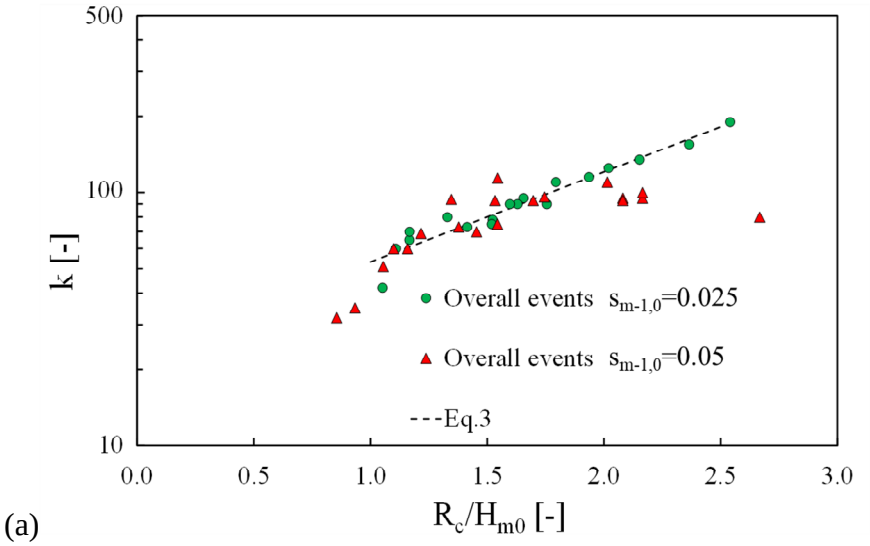

(a)

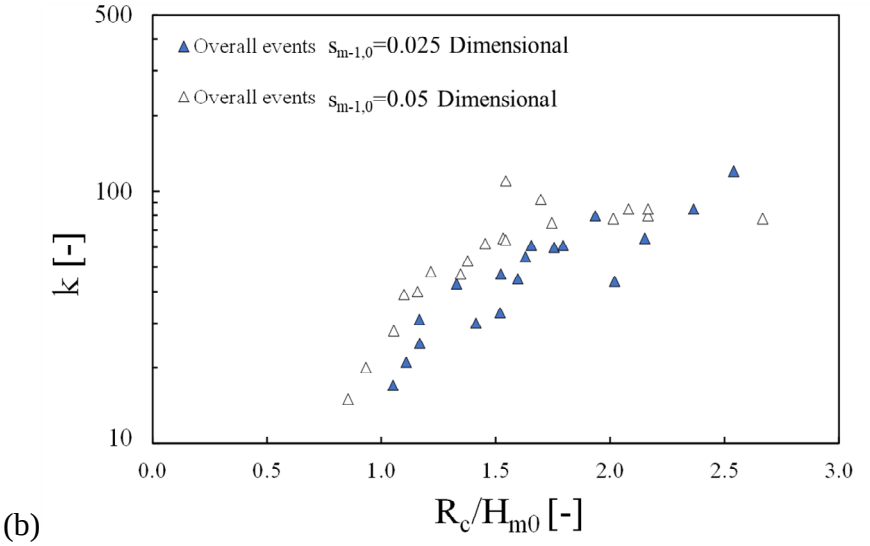

(b)

Figure 9 – Influence of incident wave steepness on the spatial distribution of wave overtopping: (a) k derived from the dimensionless relationship between q* and $x/L_{m-1,0}$, (b) k derived from the dimensional relationship between q* and x.

4.3 Travel distance of overall and extreme overtopping events

So far, this paper discussed the value of k parameter determined from the measurements for the cases with plain vertical seawall and highlighted the influence of relative freeboard and wave steepness in the spatial distribution of overtopping hazard. To undertake a systematic and comprehensive analysis of the influence of structural configurations and hydrodynamic

conditions on the spatial distribution of overtopping, travel distance of overall and extreme overtopping events is determined. It was shown that, across all the tested wave steepness, travel distance of extreme overtopping event is larger than those values determined for time-averaged spatial distributions (Figure 10). Also, it was shown that relative freeboard is also playing a key role in determining distribution of wave overtopping. Increase of freeboard was associated with a more intense increase of k parameter for extreme overtopping events. Additionally, under wave conditions with both large and small wave steepness, overtopping waves generally travelled further during extreme overtopping events with R_c/H_{m0}<1.5. With the increase in freeboard R_c/H_{m0}, the gaps between spatial distribution of extreme and total events was reduced. The scatter between the distributions extreme and total overtopping events become negligible when $R_c/H_{m0} > 2.0$.

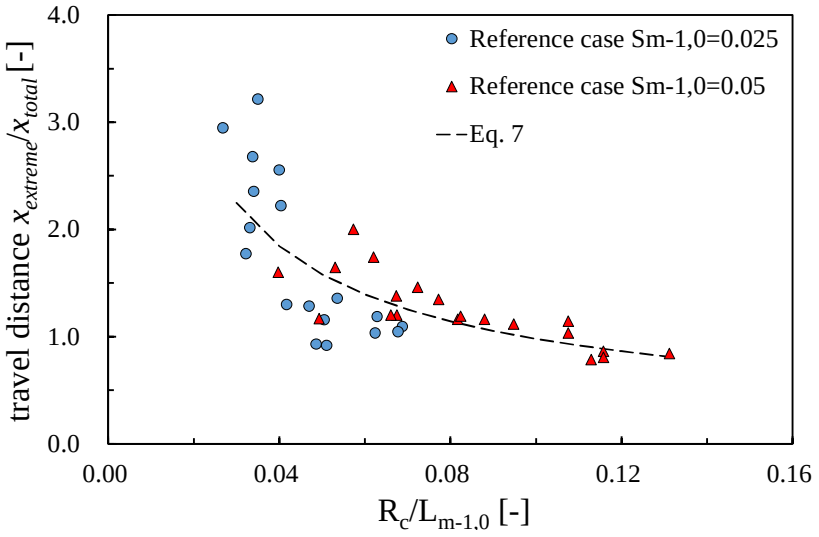

Figure 5 – Increases in travel distance for 85% of overtopping volume.

To understand the difference between spatial distributions of overall and extreme events, the travel distance of 85% mean overtopping discharge is compared with the travel distance of 85% extreme discharge. The underlying rationale behind analysing 85% proportion of overtopping discharge is the significant role it plays in determining the shape of spatial distribution. Hence, the influence of remaining overtopping discharge proportion in distribution of hazard zone is

459 negligible. The analysis of spatial distribution of overtopping volumes confirm that freeboard
460 and wave steepness affect the travel distance, and the crest freeboard takes the dominant role
461 in determining the distribution of hazard zone behind the seawall. It was shown that the travel
462 distance of overtopping waves increases when freeboard and wave steepness parameters
463 decrease. Thus, changes in travel distance are correlated with $R_c/H_{m0}\times s_{m\text{-}1,0}= R_c/L_{m\text{-}1,0}$. Figure
464 10 shows the increases in travel distance for 85% of overtopping volume. It is evident from the
465 graph that increase of $R_c/L_{m\text{-}1,0}$ results in reduction of ration of travel distance of extreme events
466 over total overtopping. Continuous increase of $R_c/L_{m\text{-}1,0}$ led to reduction of the increase ratio in
467 travel distance from around 4.0 to 1.0. This indicates that under low freeboard or low wave
468 steepness conditions, travel distance of extreme overtopping events is significantly longer than
469 the average of all the overtopping events. Increase of freeboard and wave steepness lead to
470 similar travel distance for both extreme events and overall overtopping. The findings of this
471 study confirm Peng and Zou (2011) results that larger overtopping discharge will create a larger
472 hazard zone behind the seawall. It was shown that for extreme overtopping events a more
473 significant increase in the hazard zone is expected in comparison to mean overtopping events.
474 The increase ratio in travel distance is determined from physical modelling measurements and
475 is described by Eq. 7 with an RMSE value of 0.38:

476 $$\frac{x_{extreme}}{x_{total}} = 0.2 \times \frac{R_c}{L_{m-1,0}}^{-0.69} \quad [7]$$

477 **4.4 Effects of recurve walls**

478 To mitigate the long-term challenge of sea-level rise and more extreme overtopping hazards,
479 applications of additional retrofitting structures are necessary. The performance of retrofitting
480 structures is evaluated by the enhanced mitigations they provide with reducing the wave
481 overtopping discharges. Previous studies proposed empirical-based predictive tools for
482 evaluating overtopping discharges behind recurve walls placed on the crest of sloping and

vertical structures (Pearson et al., 2004; Van Doorslaer et al., 2010). However, very limited information is provided for assessments of overtopping hazard zones behind recurve walls, which is crucial for planning coastal infrastructures and managing the risks from extreme climatic events.

This study presents physical modelling measurements of overtopping rates and the spatial distribution of overtopping events from vertical seawall with recurve retrofitting. The recurve prototypes with varying size were tested to evaluate the effects of geometrical properties of recurve structure on the distribution of hazard zone behind the seawall. The recurve walls were separately tested under both impulsive and non-impulsive wave conditions, in order to capture different overtopping processes and the structural response of recurve wall to these hydrodynamic conditions. Tests are designed to investigate the impacts of recurve's dimensions and wave characteristics on the distribution of hazard zone behind the seawall.

4.4.1 Non-impulsive wave conditions

In previous sections it was shown that R_c/H_{m0} plays a dominant role in determining the value of k for the spatial distribution of overtopping. The measurements for the cases of plain vertical seawall showed that value of k increases exponentially with R_c/H_{m0}. Figure 11 plots the dimensionless k against R_c/H_{m0} for overall overtopping events from plain vertical seawall retrofitted with three tested recurve configurations. The results for the non-impulsive wave conditions show that all measured k from recurve configurations remain above those values measured from the reference cases, indicating reduction of hazard zone behind the seawall by recurve retrofitting. On average, the travel distance of 85% overtopping discharge for the recurve retrofitting test cases reduce by 45% for the temporally averaged distribution behind the seawall. Similarly, for the case of extreme overtopping events, the recurve walls reduced the hazard zone behind the seawall by up to 53% in comparison to those cases tested for the

plain vertical wall. For recurve retrofitting cases, predictive relations are derived for the spatial distribution of hazard zone based on the physical modelling measurements. The empirical-based predictive equations are determined for the *k* parameter for both mean and extreme overtopping events from the recurve walls (Eq. 8 – 13).

Figure 11 highlights that regression lines for the three tested recurve prototypes are approximately parallel to the results obtained for the reference case of the plain vertical seawall, which led to very similar exponent values in the empirical formulae (Eq. 8 – 13) for each configuration. The location of these regression lines represent reduction in travel distance for the recurve retrofitting prototypes tested in this study. The higher the regression lines, represent a shorter travel distance of overtopping water. The findings of this study show that smallest overtopping hazard zone is observed for the case of LR, followed by HR retrofitting. Although SR resulted in the largest distribution of hazard zone behind the seawall in comparison to the other tested recurve walls, the measurements show that SR retrofitting is still effective in reducing travel distance of overtopping water, with an average reduction of 33% for overall overtopping events compared to the plain vertical seawall.

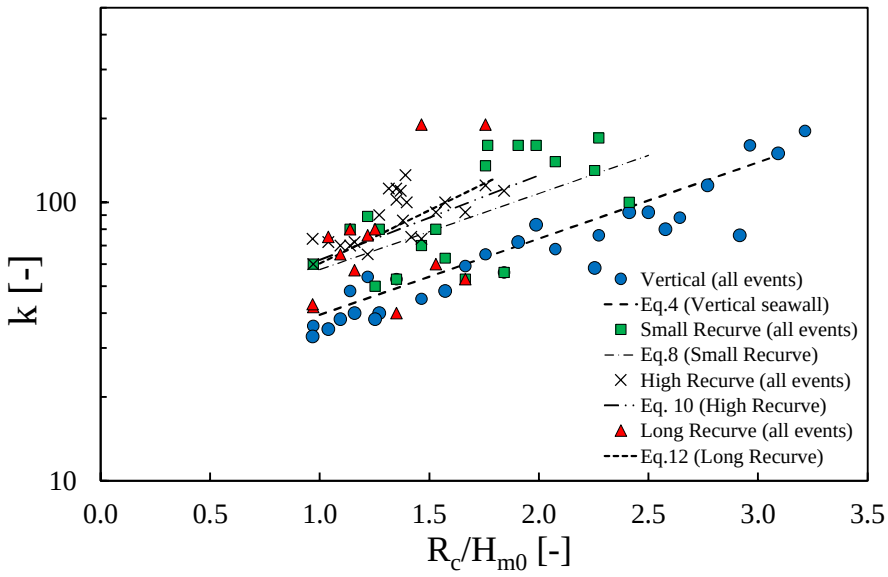

Figure 6 – Variation in spatial parameter *k* and its empirical equations for mean overtopping events from all tested configurations (Non-impulsive).

Eq. 8 – 13 present the empirical-based equations for predicting the distribution of wave overtopping hazard zone behind the seawall for the cases with recurve retrofitting. Eq. 8 and 9 are the proposed predictive relations for *k* parameter for the case of SR retrofitting for overall and extreme overtopping events, respectively:

$$k = 30.5e^{0.63R_c/H_{m0}} \quad \text{overall events} \qquad [8]$$

$$k = 12.7e^{1.02R_c/H_{m0}} \quad \text{extreme events} \qquad [9]$$

The performance of the proposed predictive relations was evaluated with statistical error index. The RMSE values for Eq. 8 and 9 are determined as 0.19 and 0.16, respectively.

For the cases of HR retrofitting, Eq. (10) and Eq. (11) are proposed for the overall and extreme overtopping events, respectively. RMSE for Eq. (10) and Eq. (11) are determined as 0.17 and 0.19, respectively.

$$k = 25e^{0.88R_c/H_{m0}} \quad \text{overall events} \qquad [10]$$

$$k = 18.9e^{0.95R_c/H_{m0}} \quad \text{extreme events} \qquad [11]$$

For the case of LR retrofitting, Eq. (12) is derived for the overall (RMSE=0.09) and Eq. (13) for the extreme (RMSE=0.17) overtopping events.

$$k = 30e^{0.7R_c/H_{m0}} \quad \text{overall events} \qquad [12]$$

$$k = 13.6e^{0.96R_c/H_{m0}} \quad \text{extreme events} \qquad [13]$$

4.4.2 Impulsive wave conditions

Analysis of the physical modelling data for the cases of recurve wall under impulsive wave conditions shows that wave-structure interactions and overtopping processes have more complicated behaviour in comparison to the non-impulsive waves, with more scatters in the recorded *k* parameter across all configurations tested. Figure 12 shows the variations of measured *k* with relative freeboard on plain vertical seawall and the three recurve walls tested under impulsive waves. The measured *k* from recurve wall configurations do not follow the empirical relationship derived based on the measurements from the plain vertical seawall. Also, evaluating the mitigating performance of each recurve prototype based on the *k* values is a difficult task. When $R_c/H_{m0} < 1.3$, most of measured *k* from all the recurve prototypes are larger than the values recorded for the reference cases. On the contrary, when $R_c/H_{m0} > 1.8$, the *k* values become significantly smaller than those *k* values measured from the plain vertical seawall, and for $1.3<R_c/H_{m0}<1.8$, the *k* values decrease sharply with R_c/H_{m0}.

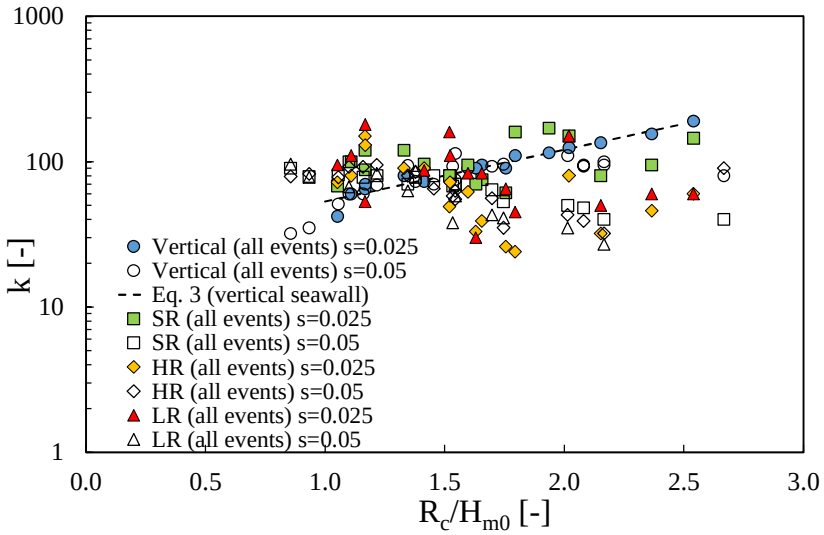

Figure 7 – Variation in spatial parameter *k* and its empirical equations for mean overtopping events from all tested configurations (Impulsive).

The differences in measured *k* parameter between the reference case and the retrofitting cases for impulsive waves, can be associated to different overtopping processes on the recurve walls.

561 The qualitative observations during the physical modelling tests show that three distinct wave-
562 structure interaction processes are present for the cases of recurve retrofitting. The first recurve
563 structure response to wave attack is the waves throw up and reflections (throw down) by
564 colliding the recurve structure. These types of waves are more likely to be returned seaward by
565 recurve wall and don't result in significant overtopping (Figure 13a). The second dominant
566 structural response was mainly observed for large incident waves, where they filled the crest
567 freeboard area in front of the wall and resulted in overflow of water from the seawall. For the
568 second types of wave attack (Figure 13b), the overtopping discharge and travel distance behind
569 the wall are attenuated due to the interactions of waves with recurve and the resulting reduction
570 in the turbulent kinetic energy of waves. The results obtained from non-impulsive wave
571 overtopping are typical example of the overtopping process shown in Figure 13b. The third
572 dominant overtopping processes happened when large incident waves collided with reflected
573 waves in front of the seawall, creating an area of a very small to no crest freeboard in front of
574 the structure (temporarily), leading into wave shoaling up and jump before reaching the toe of
575 the structure. The interactions between incident and reflected waves and the shoaling up of the
576 waves in front of the structure result in wave throw over the recurve wall and overtopping with
577 horizontal landward velocity. The test results indicate that recurve wall is capable of mitigating
578 the volume of wave overtopping for these types of waves (Figure 13c). The overflowing and
579 throw-landward waves (Figure 13c) generally result in larger overtopping volume in
580 comparison to the throw-up waves (Figure 13a).

581 For the cases with limited freeboard, waves are likely to run over the seawall though throwing
582 over or overflowing process. Those cases with recurve wall mounted on the crest of the seawall
583 have shown higher wave energy dissipation during the overtopping process, thus, less energy
584 remained for waves to moving landward during post overtopping processes. Hence, for recurve
585 retrofitting cases reductions in both overtopping discharge and travel distance were recorded.

For the retrofitting cases, where less turbulent kinetic energy was available to facilitate landward travel of the incident waves, the larger *k* parameter was measured in the cases with large overtopping level (Figure 12, $Rc/H_{m0}<1.3$). As freeboard increases, the mean overtopping discharge decreases exponentially, and it becomes more difficult for the waves to overflow. Thus, those small overtopping waves measured on the vertical wall are now attenuated or even returned seaward by the recurve wall, while relatively large overtopping events are still occurring. Discharges from those small overtopping events, which land close to seawall for the case of plain vertical seawall configurations, are completely mitigated by recurve configurations. The volumes close to seawall takes less proportion in mean overtopping volume, and therefore the *k* parameter is reduced for the recurve configurations.

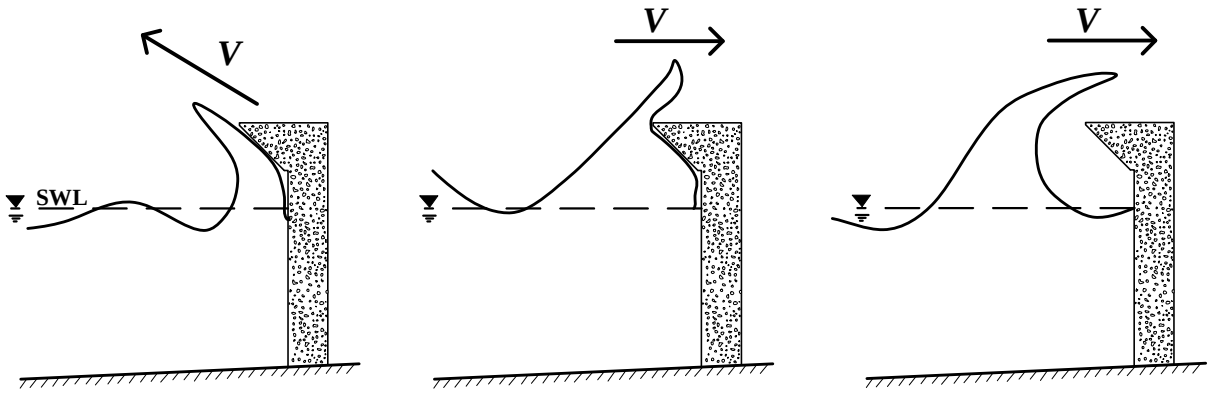

(a) (b) (c)

Figure 8 – The dominant overtopping scenarios on recurve wall (a) Throw-up waves returned seaward, (b) Overflow waves, and (c) Throw-landward waves

4.4.3 Reductions in overtopping discharges

Due to difficulties in predicting the shape of the spatial distribution of wave overtopping behind recurve walls, overtopping discharge volumes are studied as an indicator for evaluating hazard level behind recurve retrofitting prototypes. In order to provide insights into spatial distribution

603 of the risks of overtopping hazards in coastal region behind the recurve wall, analyses were
604 undertaken on the variations of overtopping discharge in different locations behind the wall.
605 The overtopping discharge reduction in coastal region is defined as the reduced overtopping
606 discharge in the total discharge measured for the reference case (RC), ($\gamma = 1 - \left(\frac{q_{recurve}}{q_{RC}}\right)$).
607 The performance of recurve walls in attenuating the wave overtopping and spatial distribution
608 of hazard zone is evaluated according to the reductions in the overtopping discharge at
609 locations behind the seawall. Such information can also help to better understand the
610 unpredictable behaviour of spatial parameter *k* under impulsive conditions.

611 Figure 14 plots the reduction in overtopping discharge in the first seven chambers of
612 overtopping measurement device (see Figure 2b) for the three recurve walls tested in this study.
613 It is found that the recurve wall configurations led to a further reduction in the overtopping
614 events with short travel distance. When R_c/H_{m0}>1.2, Comparison of overtopping discharge in
615 individual chambers highlights that a greater reduction was observed in those chambers which
616 were located immediately after the seawall (coloured data in Figure 14), with a minimum
617 reduction of at least 90% across all cases. For the overtopping discharge data recorded in
618 Chamber No. 5 and beyond, more scatters are found in the data and it was shown that recurve
619 walls have lower effectiveness in reducing overtopping events which generally lead to high
620 distribution of hazard zone. The graph shows that overtopping discharge lands after Chamber
621 No.5 (see Figure 2b) decreases by 80% as a minimum rate for LR, followed by 60% reduction
622 for SR and 40% reduction for HR retrofitting.

623

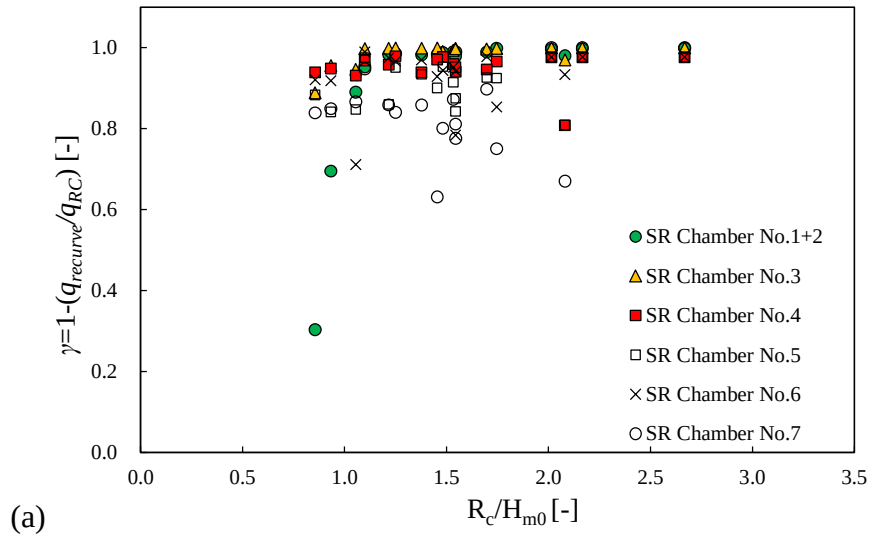

(a)

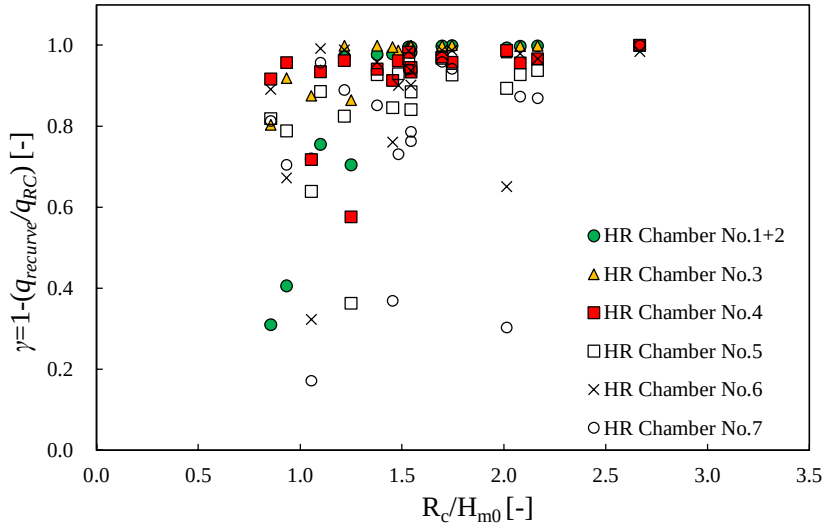

(b)

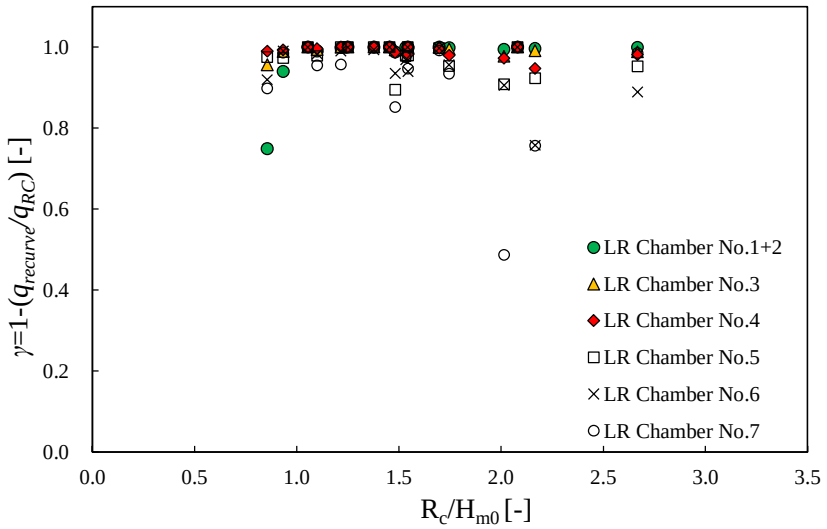

(c)

Figure 9 – Overtopping discharge reductions in the first seven chambers measured on recurve walls for (a) Small Recurve, (b) High Recurve, and (c) Long Recurve. Reduction (γ) is described as the ratio of the reduced discharge on recurve wall (q_{RC}-$q_{recurve}$) to the discharges on vertical seawall (q_{RC}) $\gamma=1-(q_{recurve}/q_{RC})$.

4.4.4 Prediction of safe zone behind the seawall

Figure 14 shows that the discharge reduction decreases as a result of the increase in the distance from the seawall (x). When the distance x exceeds the affected zone, the discharge reduction increases sharply to 100%. Based on this finding, empirical estimations of discharge reductions within the affected zone can be derived as a function of the distance x from the seawall.

Figure 15 illustrates the estimations of overtopping discharge reduction in the coastal region behind the three recurve configurations tested in this study. The distance from the seawall is normalised by offshore wavelength. $R_c/H_{m0}\times s_{m-1,0}$ is plotted on x-axis, since they play an important role in determining the reduction in wave overtopping. The graph in Figure 15 shows the relationship between $x/L_{m-1,0}$ and $R_c/H_{m0}\times s_{m-1,0}$ corresponding to two discharge reductions behind the seawall, including 95% and 80%.

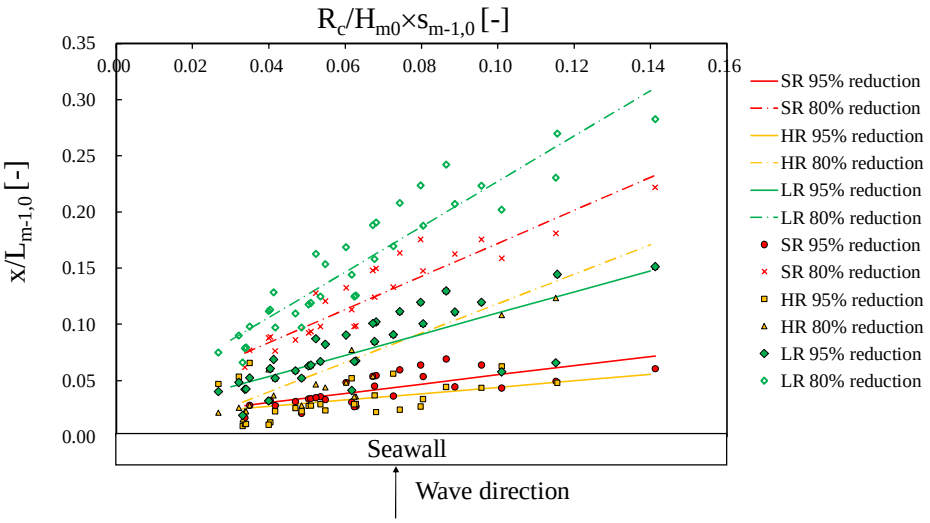

Figure 10 – Spatial variation of overtopping discharge reductions behind the vertical seawall with the recurve retrofitting prototypes

Each line in Figure 15 represents the boundary of coastal region observed with corresponding mean overtopping discharge reductions. As values of $R_c/H_{m0}\times s_{m-1,0}$ increases, the area for all the discharge reduction is found to become larger. This indicates that either higher freeboard or steeper incident waves will result in less overtopping discharge in the coastal region. The

reduction in the hazard zone behind the seawall shows enhanced level of protection provided by the coastal defence.

Due to the geometrical shape changes for the recurve retrofitting tested in this study, the reduction predicted for each recurve is different. Figure 15 shows the hazard zone behind the three tested recurve walls. Specifically, it was shown that if the overhang length is increased, reduction in overtopping will increase, and the spatial distribution of the hazard zone will shrink. Therefore, the predicting line (Figure 15) with 95% discharge reduction for the tests with LR is above the predictions derived for the SR and HR retrofitting. The results show that, for LR cases, the coastal area over which the 95% overtopping discharge decays, is the largest amongst all the tested retrofitting configurations. Conversely, increase in the height of the recurve wall led to a smaller overtopping discharge reduction. The prediction line for HR cases is below the prediction lines from the other two retrofitting configurations. Further experiments are required to extend the validation of the proposed empirical predictions for a range of recurve's shape and size.

5. Conclusions

This study presents physical modelling laboratory measurements of the spatial distributions of overtopping water behind plain vertical seawall and recurve walls with varying geometrical size. The hydrodynamic conditions were designed to cover both swell and storm conditions. The experimental tests were designed to investigate a comprehensive range of wave conditions, crest freeboard and structural configurations. An overtopping measurement system was designed for this study to enable high-resolution spatiotemporal recording of the overtopping events and spatial distribution of overtopping behind the seawall. The tests were undertaken on an impermeable smooth 1:20 foreshore slope. The overtopping volume and post overtopping spatial distribution of the overtopped water are analysed for the reference case of plain vertical

wall and the three recurve retrofitting prototypes tested in this study. The influence of hydrodynamics, geometrical shape and structural configurations on the shape of the spatial distributions of overtopping water are also analysed and discussed.

Measurements on the plain vertical seawall showed that Pullen et al. (2009) proposed predictive relations for the spatial distribution of overtopping at vertical seawalls overestimate the travel distance of overtopping water for both impulsive and non-impulsive waves. The analysis presented in this paper show that alongside the effects of wind speed and shoreward distance from the seawall, the influence of relative freeboard (Rc/H_{m0}) should be considered for robust predictions of overtopping travel distance. Considering the influence of relative freeboard on the incident wave-structure interactions and post overtopping processes, new prediction formulae are proposed for evaluating the spatial distribution of mean overtopping (Eqs. 3-4) as well as extreme overtopping events (Eqs. 5-6). The statistical analysis of the proposed predictive relations shows an overall good agreement with the measurements. The analysis of the data on extreme overtopping events shows that the overtopping water during extreme events generally travel further than time-averaged spatial distribution, highlighting the importance of evaluating hazard zone behind the seawalls for extreme climatic events.

Furthermore, the results of the tests with recurve walls show a significant reduction in the extend of hazard zone behind the seawall structure. Under non-impulsive wave conditions, parameter k (Eq. (1)) from all tested recurve walls were larger than those observed for the plain vertical seawalls. On average, the travel distance of 85% overtopping discharge was reduced by 45% for the time-averaged overtopping distribution behind all tested recurve walls. Similar findings were also observed for the extreme overtopping events, with a reduction of 53% for the travel distance of 85% overtopping discharge.

693 The analysis of physical modelling data show that increase in overhanging length, and height
694 of the recurve wall reduce the spatial extend of the hazard zone behind the wall. This study
695 develops a new and improved empirical-based formulae (Eqs. 8-13) for prediction of the *k*
696 parameter for the three retrofitting configurations tested under non-impulsive wave conditions.

697 For impulsive wave conditions, at present there is no available empirical method to predict the
698 *k* parameter for the spatial distribution of overtopping behind recurve walls. However, the
699 mitigating effects of the recurve walls for impulsive wave attack is estimated from the
700 overtopping discharge reduction at different distances behind the seawalls. Measurements from
701 the tested recurve walls highlight that a longer overhanging length enables the recurve wall to
702 provide relatively higher reduction in the spatial distribution of hazard zone behind the
703 structure, whilst increase in height of the recurve has no notable effects in reducing the extend
704 of the hazard zone.

705 **Acknowledgements**

706 This study was partially funded by the Royal Academy of Engineering – Leverhulme Trust
707 fellowship scheme. Financial support from China Scholarship Council has also helped this
708 study.

709

710 **List of Symbols**

g	Gravitational acceleration =9.81 [m^2/s]
H_{m0}	Significant wave height derived from spectral analysis = $4\sqrt{m_0}$ [m]
h_s	Water depth at the toe of structure [m]
h_*	Impulsiveness of waves, $h_* = {h_s}^2/(H_{m0}L_{m-1,0})$[-]
h	Height of the flume [m]
k	Spatial parameter as suggested by Pullen et al. (2009) [-]
$L_{m-1,0}$	Deep water wavelength based on $T_{m-1,0}$. $L_{m-1,0}=gT^2_{m-1,0}/2\pi$
L_0	Deep water wavelength. $L_0 =gT^2/2\pi$ [m]
l	Length [m]
q	Mean overtopping discharge per meter structure width [$m^3/m/s$]
q^*	The ratio of discharge lands after the distance x in total discharge [-]
q_{x/L_0}	The overtopping discharge at a shoreward distance of x/L_0
q_{total}	Mean overtopping discharge behind the seawall
R_c	Crest freeboard of structure [m]
$s_{m-1,0}$	Wave steepness with $L_{m-1,0}$. $s_{m-1,0}= H_{m0}/L_{m-1,0}$ [-]
s_{op}	Wave steepness with L_p. $s_{op}= H_{m0}/L_{op}$ [-]
$T_{m-1,0}$	Spectral period defined by m_{-1}/m_0 [s]
T_p	Peak wave period derived from time domain analyses [s]
V_w	Wind speed [m/s]
x	Shoreward distance from the seawall [m]
w	Width of the flume [m]
γ	JONSWAP spectra peak enhancement factor [-]

711

712

References

Abolfathi, S., Yeganeh-Bakhtiary, A., Hamze-Ziabari, S.M., Borzooei, S. 2016. Wave runup prediction using M5′ model tree algorithm. Ocean Engineering, Volume 112, p. 76-81. https://doi.org/10.1016/j.oceaneng.2015.12.016.

Abolfathi, S. Pearson, J. M. 2017. Application of smoothed particle hydrodynamics (SPH) in nearshore mixing: A comparison to laboratory data. Coastal Engineering Proceedings (35). ISBN 9780989661133. ISSN 2156-1028. doi:10.9753/icce.v35.currents.16.

Abolfathi, S., Dong, S., Borzooei, S., Yeganeh-Bakhtiari, A. & Pearson, J. 2018. Application of Smoothed Particle Hydrodynamics in Evaluating the Performance of Coastal Retrofits Structures. Proceedings of Coastal Engineering, 1(36). doi: https://doi.org/10.9753/icce.v36.papers.109.

Abolfathi, S., Negrini, J., and Daneshkhah, A. 2020. Prediction of Wave Overtopping from Coastal Defence Structures using Neural Networks and Ensemble Machine Learning Approach. 2020 AGU Fall Meeting, v 2020, page NH007-0014. https://ui.adsabs.harvard.edu/abs/2020AGUFMNH0070014A.

Allsop, N. W. H., Franco, L., Bellotti, G., Bruce, T. & Geeraerts, J. 2005a. Hazards to people and property from wave overtopping at coastal structures. *Coastlines, Structures and Breakwaters,* 2006**,** 153-165.

Allsop, N. W. H., Bruce, T., Pearson, J. & Besley, P. Wave overtopping at vertical and steep seawalls. Proceedings of the Institution of Civil Engineers-Maritime Engineering, 2005b. Thomas Telford Ltd, 103-114.

Andersen, T. L. & Burcharth, H. F. 2007. Travel Distance of Single Wave Overtopping volumes. *Coastal Structures 2007*.

737 Andersen, T. L., Burcharth, H. F. & Gironella, F. Single wave overtopping volumes and their
738 travel distance for rubble mound breakwaters. Coastal Structures, 2009. 1241-1252.
739 Besley, P., Stewart, T. & Allsop, N. 1998. Overtopping of vertical structures: new prediction
740 methods to account for shallow water conditions. *Proc. Coastlines, Structures and*
741 *Breakwaters, London, UK***,** 46-57.
742 Besley, P. 1999. Overtopping of seawalls, design and assessment manual. R & D Technical
743 Report W178. Bristol: Environment Agency.
744 Bruce, T., Pearson, J. & Allsop, W. 2003. Hazards at coast and harbour seawalls–velocities
745 and trajectories of violent overtopping jets. *Coastal Engineering 2002: Solving Coastal*
746 *Conundrums.* World Scientific.
747 Bruce, T., Pullen, T., Allsop, W. & Pearson, J. How far back from a seawall is safe? Spatial
748 distributions of wave overtopping. Proc. International Conference on Coastlines,
749 Structures and Breakwaters, 2005. 166-176.
750 Cheon, S.-H. & Suh, K.-D. 2016. Effect of sea level rise on nearshore significant waves and
751 coastal structures. *Ocean Engineering,* 114**,** 280-289.
752 Chini, N. & Stansby, P. 2012. Extreme values of coastal wave overtopping accounting for
753 climate change and sea level rise. *Coastal Engineering,* 65**,** 27-37.
754 De Waal, J. P., Tönjes, P. & Van der Meer, J. W. 1997. Wave overtopping of vertical
755 structures including wind effect. *Coastal Engineering 1996.*
756 Dong, S., Salauddin, M., Abolfathi, S., Tan, Z. H., and Pearson, J. M. 2018. The Influence of
757 Geometrical Shape Changes on Wave Overtopping: a Laboratory and SPH Numerical
758 Study. Coasts, Marine Structures and Breakwaters 2017. 1217-1226.
759 https://doi.org/10.1680/cmsb.63174.1217.

760 Dong, S. & Pearson, J.M., 2018. Laboratory Study of the Spatial Distribution of Extreme
761 Overtopping Events at Vertical Structures. IOP Conference Series: Earth and
762 Environmental Science, 2018. IOP Publishing, 012013.
763 Dong, S., Abolfathi, S., Salauddin, M., Tan, Z. H., and Pearson, J. M. 2020a. Enhancing
764 Climate Resilience of Vertical Seawall with Retrofitting - A Physical Modelling Study.
765 Applied Ocean Research, 103,102331, https://doi.org/10.1016/j.apor.2020.102331.
766 Dong, S., Abolfathi, S., Salauddin, M., and Pearson, J. M. 2020b. Spatial distribution of wave-
767 by-wave overtopping at vertical seawalls. Coastal Engineering Proceedings (36v). DOI:
768 https://doi.org/10.9753/icce.v36v.structures.17
769 EurOtop 2018. *Manual on wave overtopping of sea defences and related structures. An*
770 *overtopping manual largely based on European research, but for worldwide application.*,
771 Van der Meer, J.W., Allsop, N.W.H., Bruce, T., De Rouck, J., Kortenhaus, A., Pullen,
772 T., Schüttrumpf, H., Troch, P. and Zanuttigh, B.
773 Fitri, A., Hashim, R., Abolfathi, S., Nizam Abd Maulud, K. 2019. Dynamics of sediment
774 transport and erosion-deposition patterns in the locality of a detached low-crested
775 breakwater on a cohesive coast.Water, 11 (8). 1721. doi:
776 https://doi.org/10.3390/w11081721.
777 Franco, L., De Gerloni, M., Van Der Meer, J., 1994. Wave overtopping on vertical and
778 composite breakwaters. In: Proceedings of the 24th ICCE, ASCE, Kobe, Japan, pp. 1030-
779 1045.
780 Goda, Y. 2000. *Random Seas and Design of Maritime Structures*, World Scientific.
781 Goda, Y. 2009. Derivation of unified wave overtopping formulas for seawalls with smooth,
782 impermeable surfaces based on selected CLASH datasets. Coastal Engineering, 56, 385-
783 399.

IPCC 2013. *Climate Change 2013: The Physical Science Basis. Contribution of Working Group I to the Fifth Assessment Report of the Intergovernmental Panel on Climate Change,* Cambridge, United Kingdom and New York, NY, USA, Cambridge University Press.

IPCC 2014. *Climate Change 2014: Synthesis Report. Contribution of Working Groups I, II and III to the Fifth Assessment Report of the Intergovernmental Panel on Climate Change,* Geneva, Switzerland.

IPCC 2018. *Global Warming of 1.5° C: An IPCC Special Report on the Impacts of Global Warming of 1.5° C Above Pre-industrial Levels and Related Global Greenhouse Gas Emission Pathways, in the Context of Strengthening the Global Response to the Threat of Climate Change, Sustainable Development, and Efforts to Eradicate Poverty,* Intergovernmental Panel on Climate Change.

Jensen, O. J. & Sorensen, T. 1979. Overspilling/overtopping of rubble-mound breakwaters. Results of studies, useful in design procedures. *Coastal Engineering,* 3**,** 51-65.

Kortenhaus, A., Pearson, J., Bruce, T., Allsop, N. & Van der Meer, J. 2003. Influence of parapets and recurves on wave overtopping and wave loading of complex vertical walls. *Coastal Structures 2003***,** 369-381.

Liu, Y., Li, S., Chen, S., Hu, C., Fan, Z. & Jin, R., 2020a. Random wave overtopping of vertical seawalls on coral reefs. *Applied Ocean Research,* 100**,** 102166.

Liu, Y., Li, S., Zhao, X., Hu, C., Fan, Z. & Chen, S., 2020b. Artificial Neural Network Prediction of Overtopping Rate for Impermeable Vertical Seawalls on Coral Reefs. *Journal of Waterway, Port, Coastal, and Ocean Engineering,* 146**,** 04020015.

Mansard, E. P. & Funke, E. 1980. The measurement of incident and reflected spectra using a least squares method. *Coastal Engineering 1980.*

O'Sullivan, J. J., Salauddin, M., Abolfathi, S., and Pearson, J. M. 2020. Effectiveness of eco-retrofits in reducing wave overtopping on seawalls. Coastal Engineering Proceedings (36v). DOI: https://doi.org/10.9753/icce.v36v.structures.13

Pearson, J., Bruce, T. & Allsop, W. 2002. Prediction of wave overtopping at steep seawalls—variabilities and uncertainties. *Ocean Wave Measurement and Analysis (2001).*

Pearson, J., Bruce, T., Allsop, W., Kortenhaus, A. & van der Meer, J. 2004. Effectiveness of recurve walls in reducing wave overtopping on seawalls and breakwaters. *Coastal Engineering,* 4**,** 4404-4416.

Pearson, J. M. Overtopping and Toe Scour at Vertical Seawalls. Coasts, marine structures and breakwaters: Adapting to change: Proceedings of the 9th international conference organised by the Institution of Civil Engineers and held in Edinburgh on 16 to 18 September 2009, 2010. Thomas Telford Ltd, 2: 598-608.

Peng, Z. 2010. *Transformation of wave shape and spatial distribution of wave overtopping water over a coastal structure.* Ph.D, the University of Plymouth.

Peng, Z. & Zou, Q.-P. 2011. Spatial distribution of wave overtopping water behind coastal structures. *Coastal Engineering,* 58**,** 489-498.

Pullen, T., Allsop, W. & Bruce, T. 2006. Wave overtopping at vertical seawalls: field and laboratory measurements of spatial distributions. *Coastal Engineering 2006: (In 5 Volumes).* World Scientific.

Pullen, T., Allsop, W., Bruce, T. & Pearson, J. 2009. Field and laboratory measurements of mean overtopping discharges and spatial distributions at vertical seawalls. *Coastal Engineering,* 56**,** 121-140.

Salauddin, M., Broere, A., Van der Meer, J. W., Verhagen, H. J., Bijl, E., 2017. First Tests on the Symmetrical Breakwater Armor Unit Crablock. Coastal Engineering Journal 59 (4), 1-33. https://doi.org/10.1142/S0578563417500206

Salauddin, M., Pearson, J. M., 2018. A laboratory study on wave overtopping at vertical seawalls with a shingle foreshore. Coastal Engineering Proceedings, 1(36), waves.56. https://doi.org/10.9753/icce.v36.waves.56

Salauddin, M., Pearson, J. M., 2019. Wave overtopping and toe scouring at a plain vertical seawall with shingle foreshore: A Physical model study. Ocean Engineering 171, 286-299. https://doi.org/10.1016/j.oceaneng.2018.11.011

Salauddin, M., Pearson, J. M., 2020. Laboratory investigation of overtopping at a sloping structure with permeable shingle foreshore. Ocean Engineering, 197 (1), 1-13. https://doi.org/10.1016/j.oceaneng.2019.106866

Salauddin M., O'Sullivan, J. J., Abolfathi S., Pearson, J. 2020a. Extreme Wave Overtopping at Ecologically Modified Sea Defences. EGU General Assembly 2020, Online, 4–8 May 2020, EGU2020-6162. https://doi.org/10.5194/egusphere-egu2020-6162

Salauddin, M., O'Sullivan, J. J., Abolfathi, S., Dong, S., and Pearson, J. M. 2020b. Distribution of individual wave overtopping volumes on a sloping structure with a permeable foreshore. Coastal Engineering Proceedings (36v). DOI: https://doi.org/10.9753/icce.v36v.papers.54

Salauddin, M., O'Sullivan, J. J., Abolfathi, S., and Pearson, J. M. 2021. Eco-Engineering of Seawalls—An Opportunity for Enhanced Climate Resilience From Increased Topographic Complexity. Froniers of Marine Science, 8, 674630. DOI: 10.3389/fmars.2021.674630

Van der Meer, J. & Bruce, T. 2014. New physical insights and design formulas on wave overtopping at sloping and vertical structures. Journal of Waterway, Port, Coastal, and Ocean Engineering, 140, 04014025.

Van Doorslaer, K. & De Rouck, J. 2011. Reduction on wave overtopping on a smooth dike by means of a parapet. *Coastal Engineering Proceedings,* 1**,** 6.

858 Van Doorslaer, K., De Rouck, J., Boderé, T., Vanhouwe, G. & Troch, P. The influence of a
859 berm and a vertical wall above SWL on the reduction of wave overtopping. Proc.
860 Coastlab 2010, 2010 Barcelona, Spain. 10.
861 Ward, D. L., Zhang, J., Wibner, C. G. & Cinotto, C. M. 1996. Wind effects on runup and
862 overtopping of coastal structures. Coastal Engineering 1996.
863 Yeganeh-Bakhtiary, A., Houshangi, H., aAbolfathi, S., 2020. Lagrangian two-phase flow
864 modeling of scour in front of vertical breakwater. Coastal Engineering Journal.
865 doi:10.1080/21664250.2020.1747140
866 Yeganeh-Bakhtiary, A., Houshangi, H., Hajivalie, F., Abolfathi, S., 2017. A numerical study
867 on hydrodynamics of standing waves in front of caisson breakwaters with WCSPH model.
868 Coastal Engineering J, 59, 1750005-1. doi: 10.1142/S057856341750005X

869